# Manufacturing and compressive response of ultra-lightweight CFRP cores

Pablo Vitale[a], Gaston Francucci[a], Helmut Rapp[b], Ariel Stocchi[a],*

[a] Research Institute for Materials Science and Technology (INTEMA), Universidad Nacional de Mar del Plata, CONICET, Av. Juan B. Justo 4302, B7608FDQ Mar del Plata, Argentina
[b] Institute of Lightweight Structures, Universität der Bundeswehr München, Werner-Heisenberg-Weg 39, 85577 Neubiberg, Germany

ABSTRACT

Three-dimensional carbon fiber reinforced polymer (CFRP) cores are high performance ultra-lightweight materials that can reduce the structural mass of vehicles used in the transportation and aerospace industry, increasing capabilities and performance, and reducing fuel consumption. In this work, three different carbon fiber cores are obtained using an interlocking method from flat composite laminates with different geometries. The density of the cores is maintained less than 48 kg m$^{-3}$. Sandwich panels are manufactured using these cores and carbon fiber reinforced epoxy skins. Compressive properties of the sandwich panels are evaluated and the failure modes are studied. Experimental results are compared to those predicted by analytical modeling and finite element method analysis (FEM).

## 1. Introduction

Lightweight construction is one of the most efficient ways to improve performance of many vehicles or means of transport. The weight reduction is desirable to obtain the maximum payload capability, to increase the speed enhancing the driving performance, or just to reduce the fuel consumption [1]. Thus, the development of components having high stiffness and high strength to weight ratios has always been a major priority in the automotive and aerospace industry. Due to their great versatility, sandwich structures have been established as a valid candidate in minimum structural weight design [2,3]. Sandwich panels consist of two stiff skins, separated by a low-density core attaining a high cross-sectional bending stiffness. The core thickness will define the moment of inertia of the entire panel, giving an efficient structure for resisting bending and buckling loads, with little increase in weight [2]. The need for lightweight cores has stimulated the production of different polymeric and metallic foams as cores for sandwich structures [3–5]. The elastic properties of foam cores consequently depend on their relative density $\bar{\rho}$, the elastic properties of the constituent solid material and the cell topology defined as open or closed cell [6]. In many cases, these topologies do not define the deformation behavior of the studied foam and most of them are bending dominated. Compared with stretch-dominated structures of the same relative density, foam cores show lower degrees of stiffness and strength. Thereby, stretching-governed structures such as *lattice* materials with interconnected struts present a degree of stiffness more than an order of magnitude higher than that of foams made from the same constituent material [7].

A lattice material could be made from an array of struts, connected by pin-jointed or rigidly bonded edges aiming to obtain strong and stiff structures employing as less material as possible in order to manufacture a lightweight structure. In this way, open cell periodic cellular metals (PCM) have technological interest because of their highly porous structure with 20% or less of their interior volume occupied by metals, combined with highly interconnected joints. [8]

Nowadays, the properties and benefits by using composite materials like carbon fiber reinforced polymer (CFRP) are well known. More recently, researchers have been employing CFRP as raw materials to obtain lightweight lattice and honeycomb-shape structures instead of the metals traditionally used. The basic geometry of the composite lattice or honeycomb-shape material is the same than that of the metallic ones, but these structures have better performance in terms of lightweight construction.

Finnegan and Deshpande [9] employed CFRP for manufacturing pyramidal truss sandwich cores with $\bar{\rho}$ in the range 0.01–0.1, and uniaxial compressive strength in the range of 1–11 MPa increasing with $\bar{\rho}$. The pyramidal cores showed better strength performance than most known materials including aluminum lattices, metal and polymer foams, with densities less than 100 kg m$^{-3}$.

Russel and Wadley [10] manufactured and tested CFRP square-honeycomb cores. Their relative densities $\bar{\rho}$ were obtained in the range of 0.025–0.2, with three different types of cell aspect ratio. The observed peak strengths capacities were almost 10 times higher than the square-honeycomb made from 304 stainless steel of the same density.

One of the main problems of any sandwich structure is caused by

debonding phenomena, which means that the glued surface (skin-core) must be strong enough to resist shear stresses developed during the loading of the component [11]. Nowadays, the manufacturing methods of sandwich structures have improved and this mode of failure has been mitigated, specifically when the apparent glued surface is small. Finnegan and Deshpande [9] manufactured CFRP pyramidal truss sandwich cores, which were assembled into cruciform shaped slots milled into the face sheets and later bonded using epoxy adhesive. Thereby the contact nodes were reinforced with both mechanical and chemical contributions. Furthermore, George and Wadley [12] have developed hybrid CFRP truss/foam core sandwich panels combining braided carbon fiber, polymeric foams and 3D woven carbon fiber face sheets. The core was stitched to the face sheets using Kevlar® fibers before the resin infusion, attempting to reinforce the braid-face sheet nodes.

The named ultra-lightweight (ULW) materials are employed to demark those that meet the condition of very low density (below 48 kg m$^{-3)}$) and expected to be applied in future aerospace vehicles or structures. [13] In this work, novel carbon fiber reinforced composite cores for sandwich structures are designed, manufactured and tested, targeting the low-weight statement. These designs combine the low density of lattice materials and the relative high strength and stiffness of honeycomb cores. The result was square-honeycomb cores with large internal voids, resembling both lattices and honeycombs, yet being original materials more like CFRP honeycombs. The route for manufacturing the cores is described as a combination of several known material processing, some of them shown in the literature, such as the vacuum assisted resin transfer molding (VARTM) technic, followed by a water-jet cutting phase. The interlocking method fulfill the assembly stage, facilitating the making. Later, the observed compressive response and failure modes are contrasted and compared along with the analytical and numerical models for the elastic range and maximum strength. At the end of this work, the performance of the obtained panels is compared against other competitive cores and plotted on modified *Ashby-style* charts [14]. Although our main proposal is to obtain ultra-lightweight cores as different premise from other authors, when comparing our results with the literature it is observed that the materials presented here are quite competent for compressive load bearing. The comparative results can be also seen in section 7 of this work. The obtained cores are meant to be an attractive alternative to traditional honeycombs with densities less than 50 kg m$^{-3}$, representing a relatively easy to manufacture and weight efficient structural material, with various potential multi-functional applications such as the ability to support loads, heat isolation or the possibility to embed electronics and foams. Filling the cores with foams could provide several advantages, such as heat and sound insulation and also improvement of the cores' properties to impact loads, as it was reported by Mozafari et al. [15]. These authors found that deformations of foam-filled panels were significantly lower than bare ones, and also that the specific absorbed energy was higher in the case of foam filled cores. Therefore, they concluded that foam-filling is a promising way to reinforce the honeycomb core under impact loads.

## 2. Materials and methods

Composite square-honeycomb cores were built from a pre-fabricated CFRP composite sheet material. The composite laminate was cut employing a CNC water-jet cutting machine (Fig. 1a) into rectangular shapes with void spaces. The interlocking method (Fig. 1b) employed in this work follows closely a similar procedure previously proposed by Côté et al. [16] for metallic honeycombs and more recently implemented by Xiong et. al. [17]. By bonding skins to the cores, sandwich panels can be obtained, as shown schematically in Fig. 1c.

### 2.1. Materials

Composite sheets were made from plain T300-3 k, Hexcel fibers

with a 3-ply [0°, 90°] layup, with filament diameter of 7 μm, density of 1.75 g cm$^{-3}$, 230 GPa of tensile modulus and 3530 MPa of tensile strength. The employed polymeric matrix was a DGEBA (DER 383, Dow Chemicals) having an epoxy equivalent of about 183 g eq$^{-1}$ and a viscosity $\mu$ of 9000–10.500 mPa.s at 25 °C. Glycidyl aliphatic ether (Novarchem S.A.) was used as an epoxy reactive diluent, having a reactive equivalent of 255 g eq$^{-1}$. Cycloaliphatic amine was employed as hardener (Air Products and Chemicals Inc.) having an amine equivalent of 63 g eq$^{-1}$. The mixture of components showed a viscosity of (0.575 Pa.s). Finally, a 2-component epoxy adhesive (UHU plus endfest 300®) was used for bonding skins to cores resulting in a complete sandwich panel.

### 2.2. Square–Honeycomb cores design

The most suitable choice of sandwich core design depends upon the specific application. The approach of this work consists on the design of a hybrid structure with high strength and stiffness-to-weight ratio focusing on out-of-plane loading performance, having further potential by virtue of their open structure for multi-purpose characteristics.

Compared to traditional hexagonal honeycombs, square-honeycombs overcome the drawback of low in-plane stretching strength because the cell walls are orientated according the same loading plane [18].

The advantage of having voids in between unit cells potentially allow embedding electronics and foams, as well as lattice structures like pyramidal cores. The three proposed voids designs (Fig. 2a–c) deal with the loading solicitation. The catenaries cases follow the use of inverted arcs, well know and applied in architectonic constructions. Ideally, the catenary has the characteristic of being the locus of the points where the horizontal tensions are compensated and for that reason has no lateral tensions. The curve does not move towards the sides and, therefore, does not need lateral compensation. The rectangular arrays were first thought as voids with central rods, looking forward to a more restricted system in which the load capability is enhanced by the horizontal linking.

The amounts of cross-linked columns enhance the out-of-plane loading strength within the stiffness of the core. Furthermore, the number of CFRP sheets also affects the bonding surface. Thereby, the more specific brazed surface, the less vulnerable to debonding phenomena.

Another interesting issue concerning the employed CFRP core design is the relative easiness of manufacture, when the cores are compared to traditional metallic lattice materials such as pyramidal or tetrahedral geometries where cutting and bending punches as well as dies are necessary to build up the cores, followed by a welding step for attaching the face sheets.

### 2.3. Manufacturing process

CFRP composite laminates were obtained by the vacuum assisted resin transfer molding (VARTM technique. After a complete impregnation of the reinforcement, a 2-h curing stage at 393 K in an air circulating oven was carried out. The obtained laminates had a mean thickness of $t = 0.65 \pm 0.05$ mm and a density of about 1300 kg m$^{-3}$ leading to a fiber volume content of 50 ± 1%. These composite laminates were cut by a CNC water-jet cutting machine (Fig. 1a), following four different core patterns: small and big catenaries (Fig. 2a and b) and cores with two-linear arrays following a rectangular pattern (Fig. 2c). The last core pattern showed a full-walled geometry and was used as reference for comparison reasons (Fig. 2d). Slots of $t = 0.65$ mm and spacing $L = 20$ mm were cut allowing later the interlocking of the composite cell walls. In addition, some composite sheets were cut into rectangles of 25.4 mm in height and 100 mm and 200 mm in width for compressive and shear tests respectively.

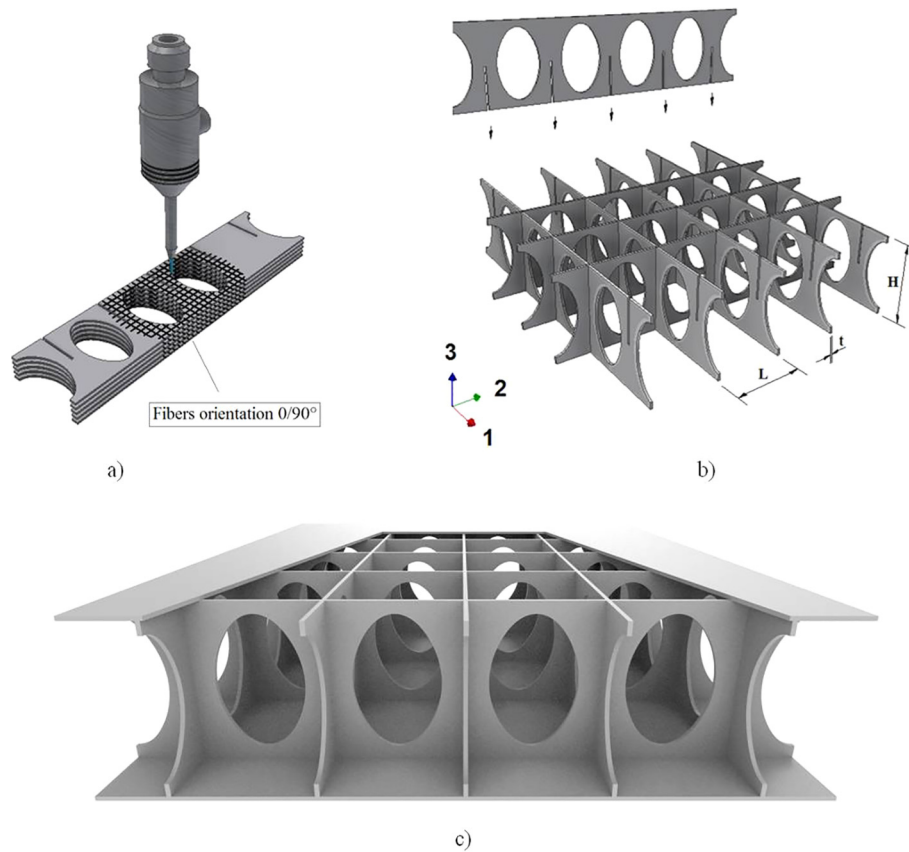Once the laminates were shaped, they were assembled by slotting

**Fig. 1.** Different rendered sketches: (a) Employed cutting method. (b) Interlocking manufacturing method. (c) Proposed sandwich panel.

together the composite sheets (interlocking method) and bonding them together with epoxy resin (same as the one used for manufacturing the composites) into a square-pattern assembly. It is important to remark that the gap between sheet thickness and slot width was about ± 0.05 mm. This clearance facilitated the assembly of the cores into a square-honeycomb pattern and also provided a suitable tight fit for stability improvement. The assembly was then placed in between pre-slotted aluminum plates with guided columns to ensure the correct position of the sheets while curing the resin at 413 K for 2 h in a heat controlled oven. Furthermore, since the rectangular sheets were not fully cured, this step was used as a post-curing stage of the parts, enhancing the bonding properties between the cross slots, due to an improved level of polymerization. Finally, the cores were bonded to CFRP face composite sheets (same as those used for the cores) employing the 2-component based epoxy adhesive. The entire assembly was then post-cured in an oven at 313 K for 24 h.

The nominal dimensions of the cores for compressive tests were 100 mm in length by 100 mm in width and a height of 25.4 mm, containing an array of 5 × 5 of 20 by 20 mm unit cells (Fig. 3a). Shear samples used the same core patterns as before, but having 200 mm in length, 100 mm in width and 25.4 mm in height. The density of each core was less than 48 kg m$^{-3}$ according to the design requirements.

The elastic properties of the core walls made from CRFP composite sheet material are specified in Table 1, considering the laminate as an orthotropic material and applying classical lamination theory for the obtained composite materials.

The coefficients $E_{is}$, $G_{ijs}$ and $v_{ijs}$ represents the elastic modulus, the shear modulus and the Poisson's ratios of the orthotropic directions as detailed in sketches (Fig. 4). The terms $\sigma_{max}$ and $\tau_{max}$ are the compressive and shear strength of the laminate, while $V_f$ correspond to the fiber volume content.
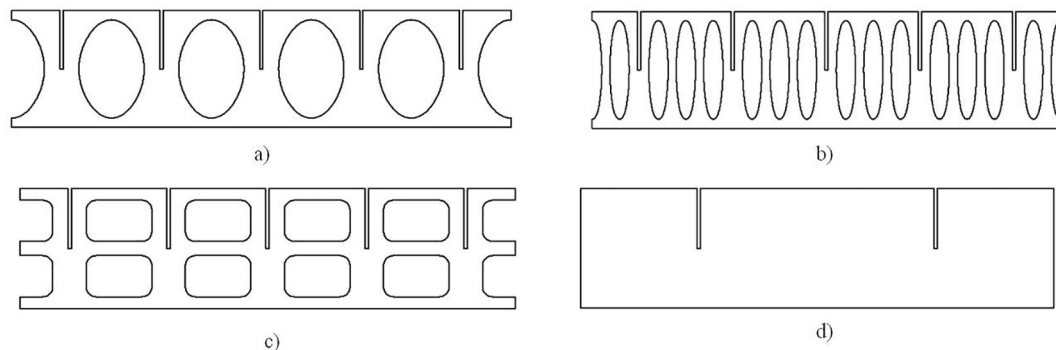


**Fig. 2.** Core patterns: (a) Design1: Larger catenaries. (b) Design 2: Smaller catenaries. (c) Design 3: rectangular array. (d) Design 4: full-walled reference.
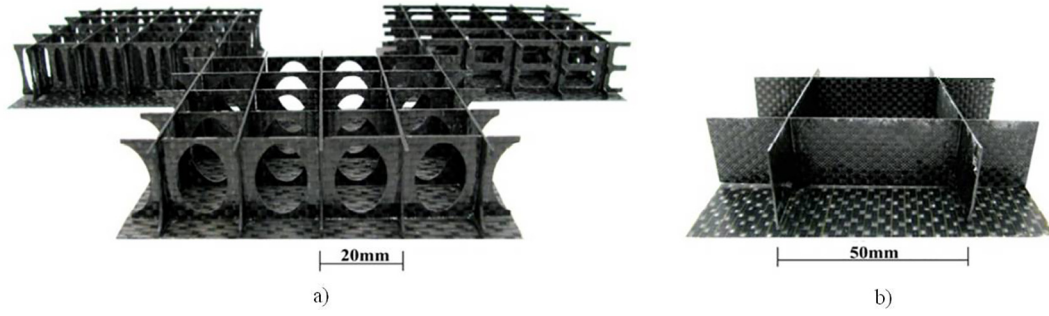
**Fig. 3.** Different geometries employed for square-honeycomb cores. (a) Proposed geometries. (b) Reference core.

**Table 1**
Theoretical elastic properties of the composite laminate material made from T300/epoxy.

| | $E_{1s}$ (GPa) | $E_{3s}$ (GPa) | $G_{31s}$ (GPa) | $\nu_{31s}$ | $V_f$ (%) | $\sigma_{max}$ (MPa) | $\tau_{max}$ (MPa) |
|---|---|---|---|---|---|---|---|
| T300/Epoxy 0/90° | 60.5 | 60.5 | 3.45 | 0.0366 | 50.8 | 1360 | 110 |

## 3. Crushing response: theory background

A honeycomb core works as spacer between the skins or face sheets. When the panel is loaded, shear and compression loads are transferred from the skins to the cores. Thereby these loads can be determined applying suitable theory concepts. Since the lightweight core consists of thin-walled plates, stability phenomenon is assumed to be the main cause of failure when compressive testing.

When the cores are loaded with an out-of-plane compressive stress, all of the cell walls are equally loaded. Often, in fiber reinforced polymer composites, failure in longitudinal compression begins by localized buckling of fibers. This behavior is due to a large difference between matrix and fiber modulus. If the matrix behaves in an elastic manner, the localized buckling mode is called *elastic microbuckling*. Applying buckling theory for columns in an elastic foundation, Rosen [19] studied two possible elastic microbuckling modes: *extension*, due to extensional strain in the matrix for low fiber volume content ($V_f < 20\%$); and *shear*, due to shear strain in the matrix. In failure prediction, it is more common to find shear strain instead of the extension mode, because most composites have more than 30% of fiber volume content. The compressive strengths of extension and shear modes are given by Eq. (1) and Eq. (2) respectively.

$$\sigma_c = 2V_f \sqrt{\frac{V_f E_m E_f}{3(1-V_f)}} \tag{1}$$

$$\sigma_c = \frac{G_m}{1-V_f} = G_{ec} \tag{2}$$

Both equations depend on the fiber volume content. Nevertheless, shear mode predicts a compressive strength lower than the extension mode. The other presented factors are the matrix shear and elastic modulus, $G_m$ and $E_m$. Factor $E_f$, denotes the longitudinal elastic modulus of the fibers while factor $G_{ec}$ represents the effective shear modulus of the composite. However, Rosen's models assume perfect conditions when balancing the strain energy change to the work done by the external forces. Thus, failure prediction stated by the models shall differ from experimental data.

On the other hand, another localized buckling mode could be expected as *fiber kinking*. Rosen [19] assumed kinking as a manner of elastic shear buckling. Therefore, kinking is presented as an elastic bifurcation buckling phenomenon and could appear in originally straight fibers. However, Argon [20] stated that long fibers under compressive loads shall buckle due to a critical compressive load and proposed a rigid-perfectly plastic composite model (Eq. (3)), including a region of initial misalignment angle $\bar{\phi}$ and the interlinear longitudinal shear
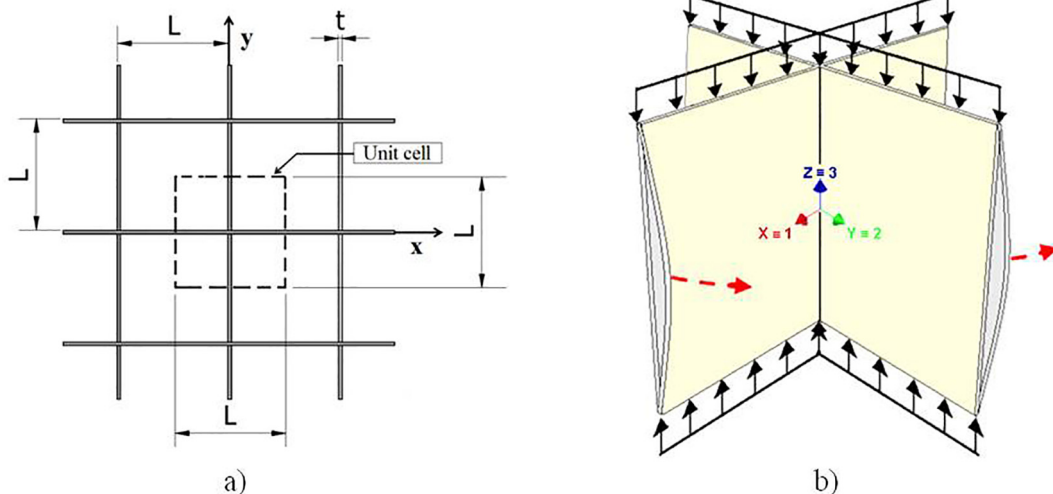


**Fig. 4.** Sketches of unit cells. (a) Unit cell employed for analyses. (b) Thin-walled cross-shape column showing torsional buckling behavior.

strength $k$. When the applied compressive stress produces an interlaminar shear component and equals $k$, it produces a local instability favored by the misalignment angle and followed by a shear collapse band.

$$\sigma_c = \frac{k}{\overline{\phi}}\tag{3}$$

Later, Budiansky [21], Budiansky and Fleck [22] determined the stress at which kinking is initiated, joining both Rosen's and Budiansky's models easily recognizable when $\overline{\phi}$ takes small or large values. Budiansky based the kinking behavior of the fibers on an elastic-ideally plastic composite (Eq. (4)), including $\gamma_{yc}$ as the shear yield strain of the composite. One of the final statements was that carbon fibers in an epoxy matrix tend to fail in compression by plastic kinking.

$$\sigma_c = \frac{G_{ec}}{1 + \frac{\overline{\phi}}{\gamma_{yc}}}\tag{4}$$

Micromechanics allow researchers to study microbuckling under axial compression of aligned-fiber composites and thus find the critical compressive peak load $P_c$. Besides elastic microbuckling and fiber kinking presented as dominant failure mechanisms on compressive loading, other competing failure modes were analyzed for this work considering the macromechanics. As a result, the other expected compressive failure mode is elastic torsional buckling. The main response of the core could be analyzed from a simplified model considering just a defined unit-cell (Fig. 4a).

In this way, under uniform out-of-plane compressive loads and considering equally loaded sizes, thin walled-columns will buckle in a torsional manner. In other words, each flange buckles by turning around the vertical axis (z-axis); while the vertical axis remains straight (Fig. 4b). The red arrows shown in Fig. 4b symbolize the turning tendency of the flanges.

Square-honeycomb columns are considered as bars of cruciform section with four identical flanges of thickness t = 0.65 mm and a width of 0.5L. The analysis proposed by Timoshenko [23] was used for evaluating torsional buckling. In this case, the shear center coincides with the centroid (Fig. 5b) and applying appropriate border conditions satisfied by sinusoidal solutions, the simplified equations are shown as follows (Eq. (5), Eq. (6) and Eq. (7)). It was considered that the cores were made from an orthotropic composite material for the analysis.

$$P_x = \frac{\pi^2 E_{3s} I_x}{H^2}\tag{5}$$

$$P_y = \frac{\pi^2 E_{3s} I_y}{H^2}\tag{6}$$

$$P_\varphi = \frac{A}{I_o}\left(C + C_1 \frac{\pi^2}{H^2}\right)\tag{7}$$

Where $P_x$ and $P_y$ are critical loads due to Euler buckling behavior, about x and y axes, respectively and $P_\varphi$ denotes the critical load for torsional buckling. Coefficient $C_1 = EC_w$ is called *warping* rigidity, $E$ is the elastic modulus of the column material and $C_w$ is called the warping constant.

$C_w$ is equal to zero for cruciform cross sections. $I_o$ is the polar moment of inertia of the cross section about shear center [0;0;0], coinciding in this case with the centroid. Coefficient $C = GJ$ is the torsional rigidity, where $G$ is the shear modulus and $J$ is the torsion constant. For open-walled sections $J = 1/6Lmt^3$ being $m$ the number of flanges. Coefficient $A$ is the cross-sectional area and $H$ is the height of the core.

Due to the involved geometries under uniformly compressed loading, elastic buckling of rectangular plates shall appear, especially for the reference cores. The formula presented by Ericksen [24] was used for evaluating elastic buckling of plates (Eq. (8)):

$$P_b = \frac{K\pi^2 D}{B^2}\tag{8}$$

$$D = \frac{\sqrt{E_{1s}E_{3s}}}{\lambda}\left(\frac{t^3}{12}\right)\tag{9}$$

$$K = 0.75\left(\frac{H}{L}\right)^2 \sqrt{\frac{E_{1s}}{E_{3s}}} + 2\alpha + 8.2\left(\frac{L}{H}\right)^2 \sqrt{\frac{E_{1s}}{E_{3s}}}\tag{10}$$

$$\alpha = \frac{1-\lambda}{\sqrt{E_{1s}E_{3s}}}\left(\frac{E_{1s}v_{31s}}{1-\lambda} + 2G_{13s}\right)\tag{11}$$

Coefficient $D$ represents bending stiffness of thin composite cell wall and it depends on the thickness $t$, Poisson's ratio $\nu$ and the Young's modulus $E$ according to 1 and 3 directions plotted on Fig. 4b. Stiffness $D$ shall be written as Eq. (9) for orthotropic composite materials. Factor $\lambda$ shall be written as $\lambda = 1 - v_{13s}v_{31s}$. Factor $B$ represents the length of the loaded edge. Coefficient $\alpha$ in Eq. (11) depends on shear modulus $G$, Poisson's ratio and Young's modulus of the composite.

It is important to remark that Eq. (5), Eq. (6) and Eq. (8) follow the same basic mechanics, but Eq.8 is specified in this case for composite materials.

Finally, the failure mechanism will be determined by the one that demands the lowest payload and thereby will determinate the critical load $P_{crit}$ (Eq. (12)) followed by the peak compressive stress.

$$P_{crit} = m(P_c, P_b, P_\varphi)\tag{12}$$

On a first approach, the potential failure modes were evaluated, resulting torsional buckling as the mode with higher probability to occur, due to the laminate mechanical properties, architecture and geometry of the cores, leading to lower critical loads.

The elastic modulus $E$ of the square honeycombs originally could be set by Eq. (13).

$$E = \overline{\rho}E_{3s}\tag{13}$$

However, since the density of the cores was nearly constant among them, Eq. (13) shall only be applied for the reference cores, where the unit-cells walls are filled with material. Then, in order to evaluate the Young's modulus of the other cores it was necessary to set each case according to the rule of mixtures, considering the amount of material that effectively carries the payload.

## 4. FE modeling

The entire evaluation of the square-honeycomb cores was resumed into a simplified case, employing unit-cells (Fig. 5), which dimensions are shown in Table 2. Unit-cells are symmetrical according to orthotropic reference axles (Fig. 4). This characteristic has many technological advantages such as an easier core design and manufacture, and a real advantage while performing finite element analysis (FEA). In this way, computational models that simplify bigger structures could be employed to predict the behavior of the whole assembly, saving computing time and the amount of modeling elements by reducing the degrees of freedom (DOF). Nevertheless, the accuracy of the analysis can be enhanced due to a simplification in the mathematics of the solution, decreasing the numerical discrepancy while computing the system [25].

Software FEMAP™ 10.3 with NX™ Nastran® [26] was employed for the finite element analysis. The proposed cores under compressive and shear loading were modeled as a single and a two-material system respectively.

Compressive tests were modeled using a single unit cell for each core case simulating the loading case according to standards [27]. Simulations were performed using different geometries of cores previously shown. Unit cells were discretized using regular mesh of shell elements (S4R) with five integration points and a size of about 0.4 mm, representing the geometry of the studied cores. In this way, shell elements dramatically reduce the complexity of modeling, as well as the computing time, while still providing good predictions for thin-walled
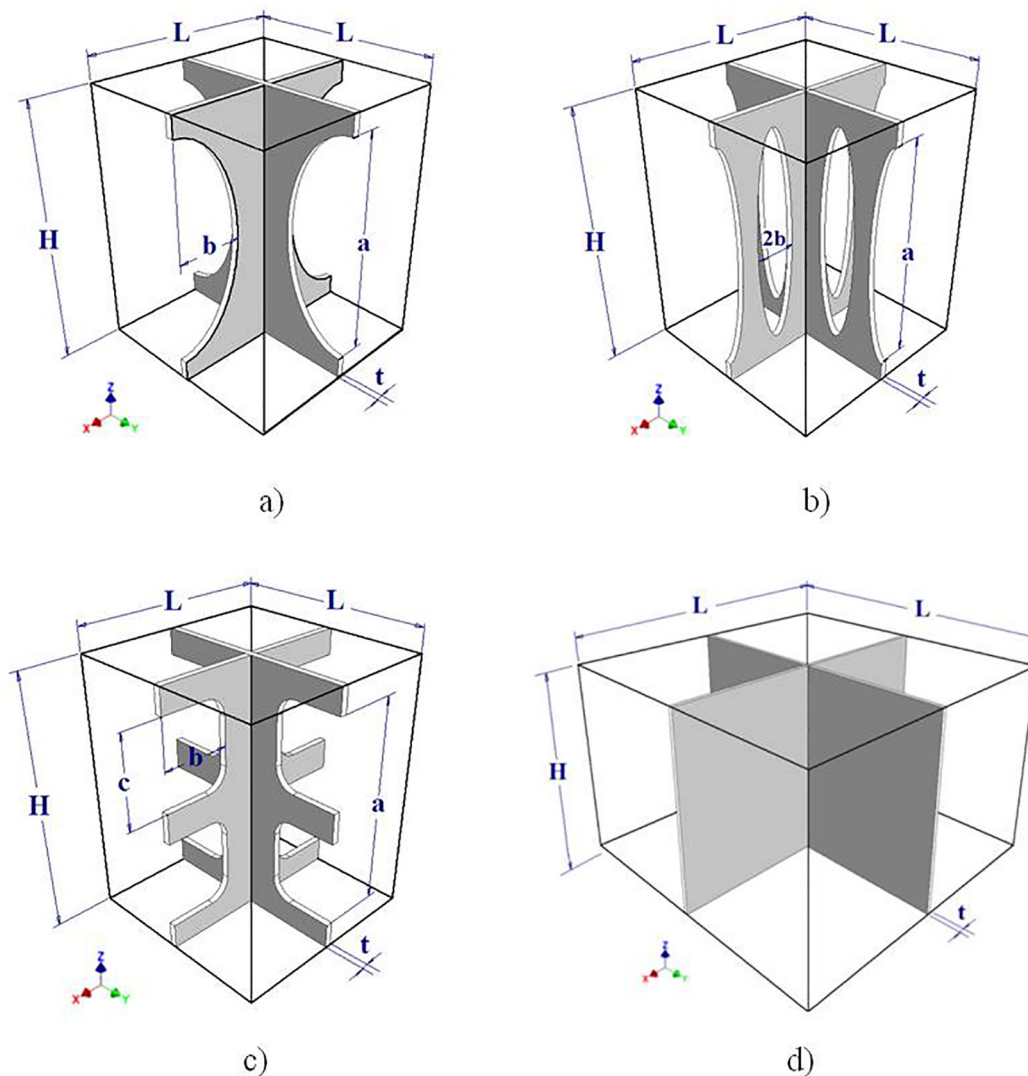
Fig. 5. Sketches of the repetitive unit cells from the presented square-honeycombs. (a) Design 1: Large catenaries. (b) Design 2: Small catenaries. (c) Design 3: Two linear rectangular array. (d) Reference.

**Table 2**
Unit-cells mean dimensions in mm employed for analyses: designs 1, 2 and 3, and reference.

| | H | L | t | a | b | c |
|---|---|---|---|---|---|---|
| Design 1 | 25.4 | 20 | 0.65 | 21.4 | 6.54 | – |
| Design 2 | 25.4 | 20 | 0.65 | 21.4 | 2.05 | – |
| Design 3 | 25.4 | 20 | 0.65 | 20.4 | 6.61 | 8.70 |
| Reference | 25.4 | 50 | 0.65 | – | – | – |

structures behavior, compared to 3D solid elements [28].

## 5. Compressive tests

Compressive tests were performed on a Zwick/Roell Z150 screw-driven universal testing machine, with an additional displacement transducer HBM W2TK. Six tests were conducted on each of the stabilized square-honeycomb core specimens in order to confirm the repeatability of the results.

Typical compressive stress versus strain response of design 1 cores is plotted in Fig. 6; while Fig. 7 represents an array of photographs at selected values, giving evidence of the behavior of the core against compressive loads. The initial response of the core is almost linear up to
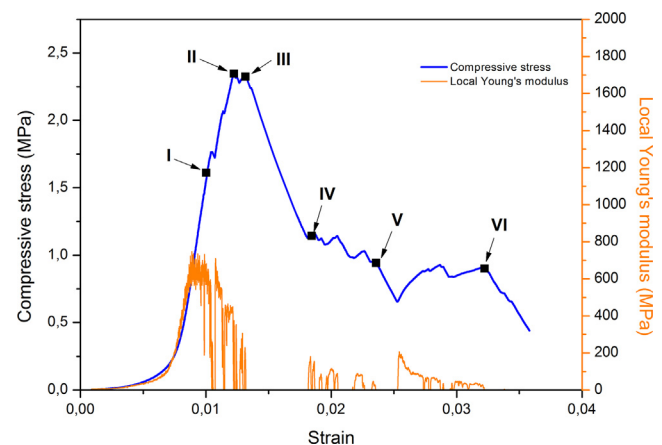


Fig. 6. Measured compressive stress–strain response of design 1 cores.

the peak stress, with a small loading drop after point I, suggesting a misalignment between the loading plates.

Then the loading slope changes gradually before reaching the maximum compressive strength of the cores, and potentially implying a case of elastic buckling of the CFRP structure. Furthermore, this
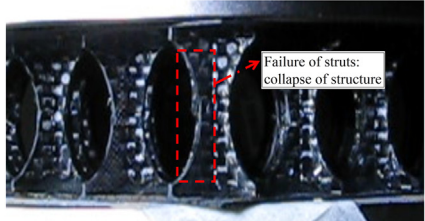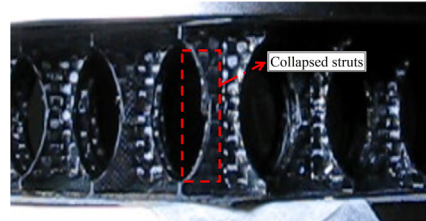
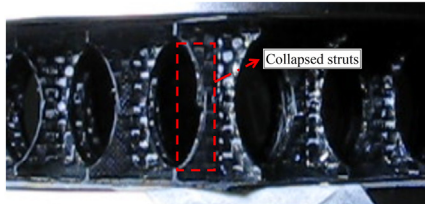Point I = (0.0100; 1.6113)
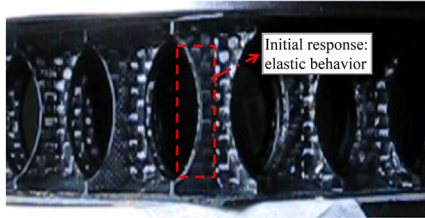
Point II = (0.0122; 2.3459).
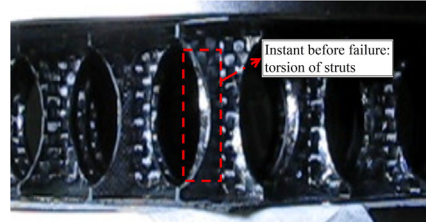
Point III = (0.0132; 2.3254)

Point IV = (0.0185; 1.1440)

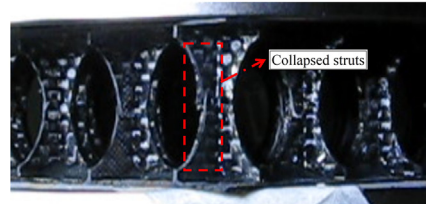Point V = (0.0236; 0.9429)

Point VI = (0.0322; 0.9007)



**Fig. 7.** Photographs associated at selected points: compressive behavior of design 1 cores.

statement is supported by the change of the local Young's modulus (Fig. 6). Later the collapse of the core occurs when the maximum loading capability is reached. The loading drop is not abrupt but it is gradual, assuming a failure due to a case of elastic buckling. [12]. This statement is evidenced by point II (Fig. 7) before the collapse of the cores, denoting torsional buckling behavior in agreement with the analytical prediction, as it will be shown in the following section. After the main drop, the stress reaches a plateau by local opposition of the crashed struts and later the stress keeps dropping with further crushing. Finally, local failure events happen progressively leading to a decrement on the global strength of the cores, following a nonlinear regime due to the subsequent collapse of the struts.

The obtained compressive stress $\sigma_{33}$ vs. strain $\varepsilon_{33}$ responses of the
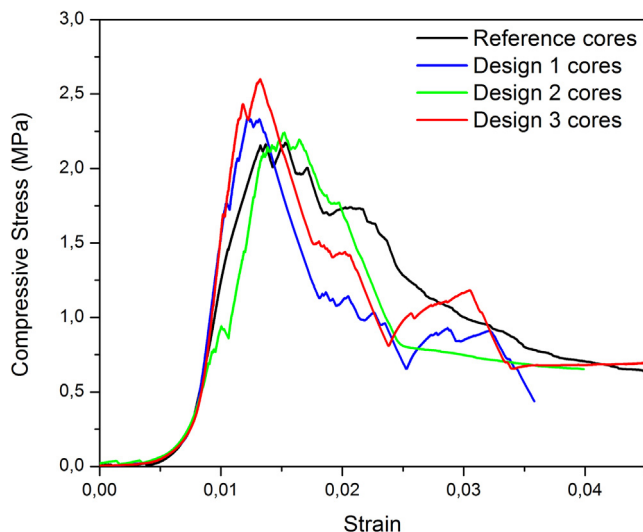


**Fig. 8.** Compressive stress–strain response of square–honeycomb cores.

proposed cores is shown in Fig. 8. The curves show in all cases an elastic response at the beginning of the tests, with a small change of the loading slope prior to the collapse of the structures, denoting the initiation of elastic buckling of the CFRP structures. After the peak, in all cases the stress falls progressively with until a plateau is reached. Then, the stress continues its decrement with further crushing.

The discrepancy among the curves indicates that the geometries may influence the main response of the cores during compressive loading. As it can be seen in Fig. 8, design 3 showed the best compressive strength performance compared to the others. However, the maximum compressive strength of the proposed cores were close to that of the reference core, even though the elastic modulus of all of the designed cores were higher than the reference. This was attributed to the higher number of struts.

## 6. Model validation

Analytical and numerical models considered a single cross-shaped structure attached to two rigid flat plates. Thereby, the struts are thought as equally loaded cross-shaped columns. Prior to collapse, the struts experiment an elastic buckling behavior in all cases. The core failure hypothesis of torsional buckling is confirmed by the contrast of the measurements with the analytical and numerical results.

Table 3 summarizes the results obtained from compressive tests. It can be seen that the failure load (F) and thus the compressive strength of the cores (see Fig. 9), were moderately over estimated, but predicted reasonably accurately by the analytical and numerical results. However, the models over estimated (two to three times) the Young's modulus of the cores, which was attributed to imperfections in the manufacturing process. Moreover, the elastic modulus shows good agreement between the analytical and numerical models but a large discrepancy compared to the experimental results. Generally speaking, the measured stiffness data in compression are, in many cases, lower than the theoretical ones because of imperfections in the test sample.

**Table 3**
Experimental, analytical and FEM results from compressive tests.

| | $F_{peak}$ (kN) | $F_{theory}$ (kN) | $F_{FEM}$ (kN) | $E_{peak}$ (GPa) | $E_{theory}$ (GPa) | $E_{FEM}$ (GPa) |
|---|---|---|---|---|---|---|
| Reference | 22.30 ± 0.25 | 27.43 | 27.01 | 0.54 ± 0.02 | 1.57 | 1.57 |
| Design 1 | 22.03 ± 1.77 | 29.16 | 29.67 | 0.72 ± 0.02 | 1.61 | 1.60 |
| Design 2 | 20.97 ± 1.03 | 30.53 | 30.39 | 0.61 ± 0.01 | 1.90 | 1.92 |
| Design 3 | 26.07 ± 1.58 | 28.69 | 28.86 | 1.12 ± 0.01 | 1.34 | 1.39 |
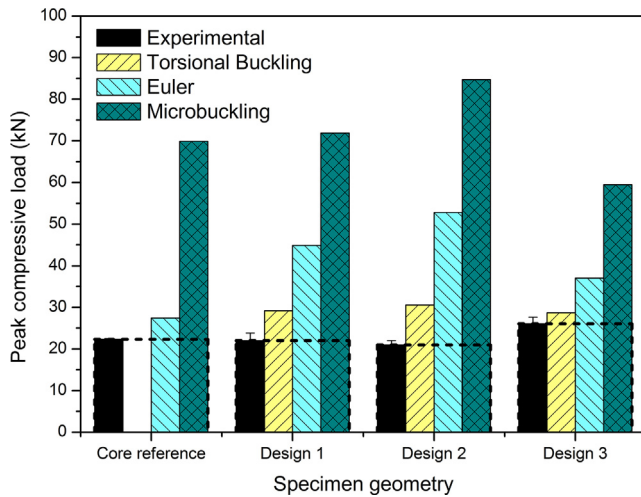


Fig. 9. Comparative peak compressive loads among different theory proposals.



Fig. 10. Maximum compressive stresses according to analytical, FEM and experimental data.

They cause out-of-plane deformations that are not consider in classical geometric linear analyses. Furthermore, since the sandwich panel samples are not ideally flat, the compression loads are not perfectly distributed over the faces. These issues are potentially though as the reasons that leads the response of the cores to deviate from the ideal situation. It is important to notice the great potential loading capabilities of the cores, considering an ideal material processing. Among the different failure proposals, it is clearly seen that the lowest estimated failure load is attributed to torsional buckling (Fig. 9) when comparing calculations with experimental data. However, special care should be taken when torsional buckling theoretical background is applied. For instance, the reference cores do not satisfy the necessary conditions specified for pure torsional buckling behavior (not considered in Fig. 9), although they experiment a certain Euler buckling mode. In this particular case, the unit cells do not compliment the conditions over the mid-plane of the flanges, coincident to point (0; 0; 0), because they are not allow to experiment rotation on the edge faces, despite being allow to displace over xy-plane. It is remarkable that all of the tested cores do showed a macro-mechanical behavior, when comparing the results with micro-buckling background.

Fig. 10 compares the maximum measured compressive strength among the proposed square-honeycomb cores. The upper bound of the experimental results is in good agreement with the analytical and numerical predictions. The variability among the results is attributed to several factors, mostly related with the fibers misalignments during the manufacturing process and the loading set-up. In all cases, the first stage of the mechanical responses was elastic followed by a buckling failure. Nevertheless, the maximum compressive strength given by the analytical models and also the numerical results evidenced on Table 4 reinforce the torsional buckling supposition.

Table 4 compares the experimental tests of the three proposed cores and contrasts them among their respective numerical result. The first column shows the augmented photographs of singles struts with a white straight line, focusing on the initial position of the sample at the beginning of the compressive test. The second column shows the instability of the struts an instant before collapse of the structure. The red
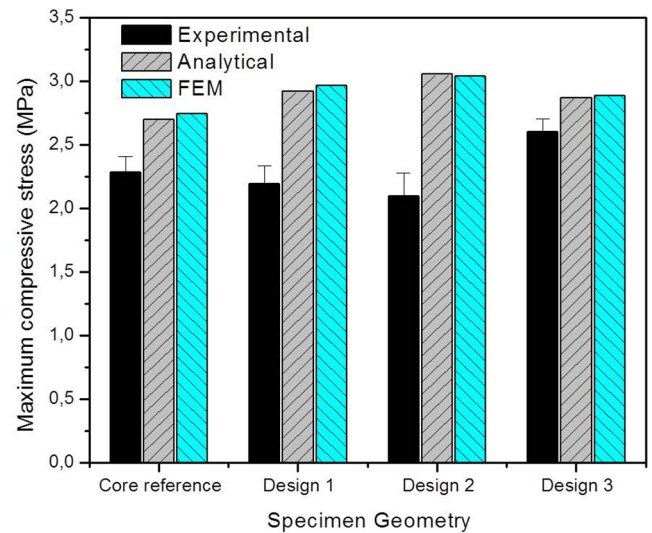
lines help to define and contrast the shape of the laminate during this stage. The third column presents FEM sketches of the unit-cells showing the instability of the struts. The failure resembled torsional buckling behavior and thus saving the proposed hypothesis. Besides, Fig. 11 shows a FEM render with 4 unit-cells working together when the core is subjected to compression loads. The red arrows help to see the turning tendency when the struts reach the instability load.
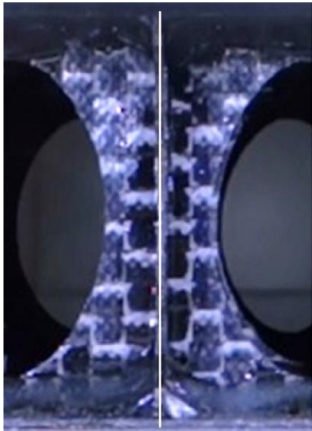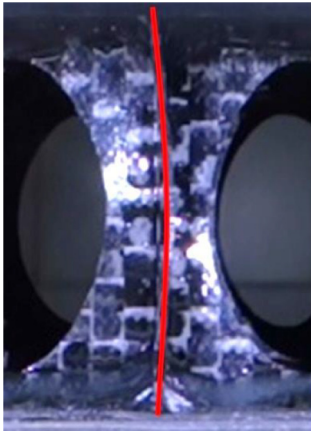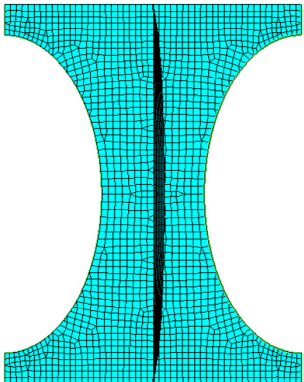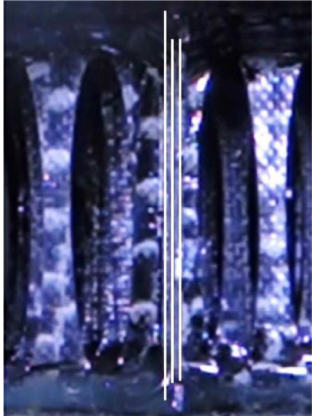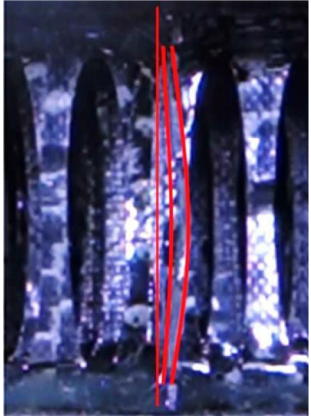
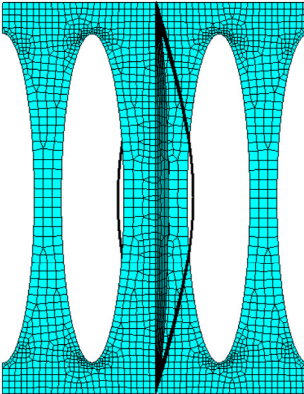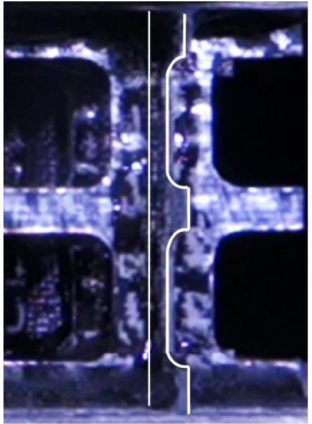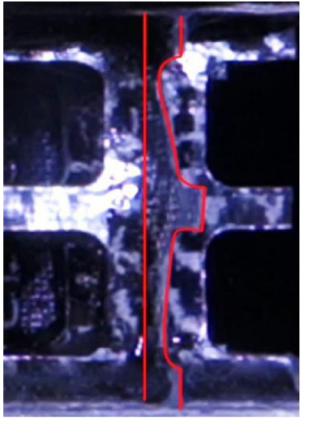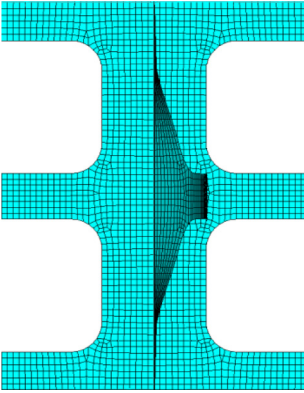Nevertheless, taking a closer look to Table 4 positions (b;2) and (b;3), the small columns at the sides of the main cross-shaped column experiment Euler buckling before the main collapse of the structure due to the slenderness of the struts. This premature elastic buckling of thin plates reduces the loading capability of the cores; thereby for this particular case, the involved calculations contemplated the sum of both effects into the unit-cell: premature Euler buckling of the small lateral columns coupled to torsional buckling of the cross-shaped column was taken into account (see Eq. (7) and (8)). This effect can be seen as well on the non-linear analyses made from the FEM analyses that support this statement. (Fig. 12)

## 7. Comparison with similar materials

In order to compare the mechanical properties of materials, Ashby and Bréchet [14] have proposed the material-property charts for engineering materials (Fig. 13. Many authors aimed to fill the gaps between existing and unattainable materials from the maps by making hybrid materials. By this means, an increasing interest exists in ultra-light cores for weight sensitive structures [29]. Fig. 13 includes compressive data for CFRP honeycomb cores [10], CFRP pyramidal lattices [9], titanium matrix lattices [30], aluminum tetrahedral lattices [31], stainless steel honeycomb cores [16] and different metallic foams [3].

In this work, the measured mean peak compressive strength of design 1 cores was chosen for comparison reasons (Fig. 13), rectangular-shape point). Design 1 cores are comparable and competitive to tradi-tional square honeycomb CFRP cores with densities less than

**Table 4**
Comparison matrix of unit-cells during loading. *Rows*: (a) Design 1 samples. (b) Design 2 samples. (c) Design 3 samples. *Columns*: (1) Photographs at the beginning of compressive test. (2) Photographs an instant before failure. (3) FEM renders of unit-cells.



$50 \, \text{kg m}^{-3}$. For instance, they have almost the same strength of the plotted Ni-foam but having four times less density. Also, compared with metal and polymeric foams, design 1 cores show better compressive performance than most of them. Nevertheless, the working temperature of the thermo-set matrix of design 1 cores allows the structure to work at a higher temperature than the commonly used polymers applied to foams.

Furthermore, Table 5 contrasts and resumes the experimental results obtained in this work with those reported in the literature. The ULW hybrids developed have better specific compressive modulus than plenty of the known metallic foams and others high performance CFRP materials, yet challenged by metallic lattices such as the AISI 304 square-honeycomb cores of similar $\bar{\rho}$, but even ULW have superior

modulus of over 54%. The diamond titanium based lattices have more than 16% better modulus, but with 274% more mass.

Even though when the pyramidal CFRP based and the tetrahedral AA6061 based lattices with nearly $\bar{\rho} = 3.5\%$ are compared with ULW hybrids, they present better compressive strength, in this terms more than 2 and 1.3 times respectively, but a lack in elastic modulus of about 3.1 and 5.7 times respectively.

The specific properties defined in terms of compressive modulus and strength demonstrates the competitiveness against other materials of similar relative density.

The proposed hybrid cores in this paper do not achieve the full potential of the predicted load capability. If the maximum theoretical load is reached by mitigating the defects introduced by the
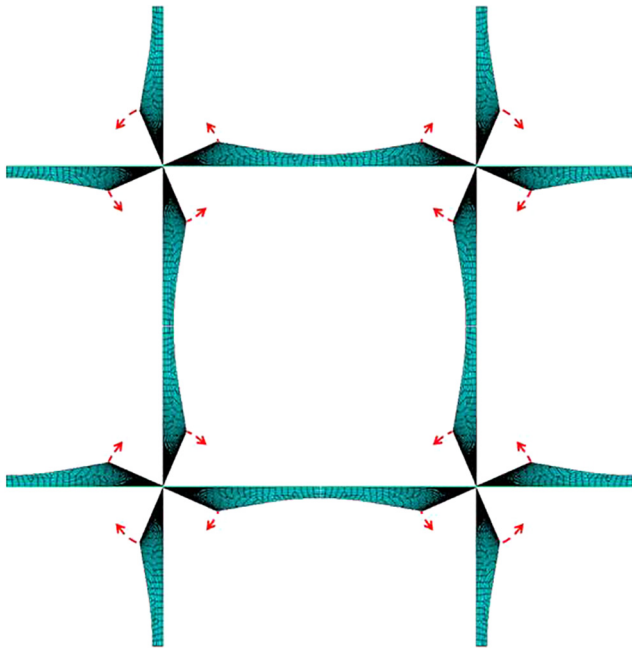
Fig. 11. FEM renders of 4 unit-cells made from design 1 struts showing torsional buckling.



Fig. 13. Material–property charts for engineering materials. Out-of-plane compressive strength as function of density. (Green rectangular-shape point = design 1, Green triangular-shape point = estimated with mitigation of manufacturing effects. (For interpretation of the references to colour in this figure legend, the reader is referred to the web version of this article.)

manufacturing processes (Fig. 13, triangular-shape point), the studied CFRP cores could be juxtaposed to the center region of pyramidal CFRP lattices but having less manufacturing steps and more bonded surface, being relevant issues for sandwich structures applications. The theoretical calculations revealed the capabilities of the proposed CFRP cores, being promising candidates for ultra-light weight applications.

## 8. Concluding remarks

Three different geometries of square-honeycomb cores were manufactured with a density below 48 kg m$^{-3}$. The compression response of each core was evaluated and compared to that of a full-walled reference core. Analytical and numerical models were developed and their predictions were compared to the experimental findings. FEM models were in excellent agreement with the analytical calculations. In all cases, the experimental strength was lower than the predicted one, while the stiffness was substantially lower than the one given by the models. The disagreement between experimental results and model predictions was attributed to imperfections in the manufacturing process of the main laminate composite material and the possible unequal load distribution of the test set-up.

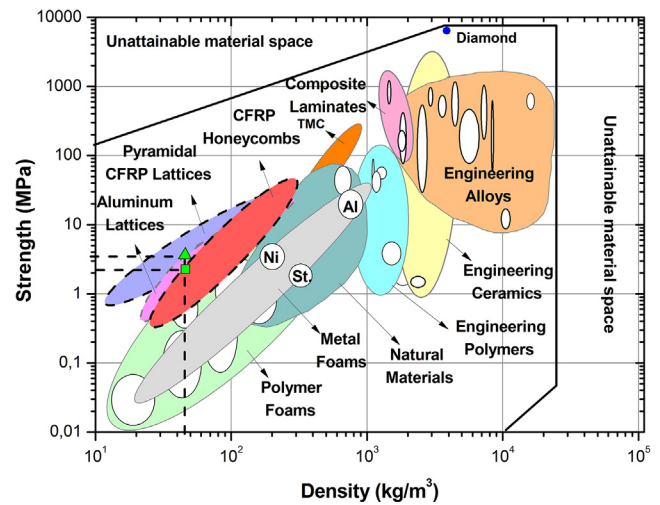The reported manufacturing method, mechanical measurement and

modeling provide a first step for developing new cores for lightweight design, attempting to expand the strength-density chart for honeycomb cores. The obtained cores showed great potential as competitive materials to most of the known polymeric and metallic foams. In addition, hollow cores with interconnected void spaces as the ones manufactured in this work present further advantages, as the ability to be used on multifunctional applications (for example the possibility to embed electronics and foams). The interlocking method using reinforced polymeric materials showed to be a feasible production method to obtain light-weight competing materials for sandwich applications. This method has many advantages related to the ease of processing compared to conventional methods [32].

Furthermore, the square-honeycomb cores with high number of arrays have more specific bonded surface, making them less vulnerable to debonding phenomena.
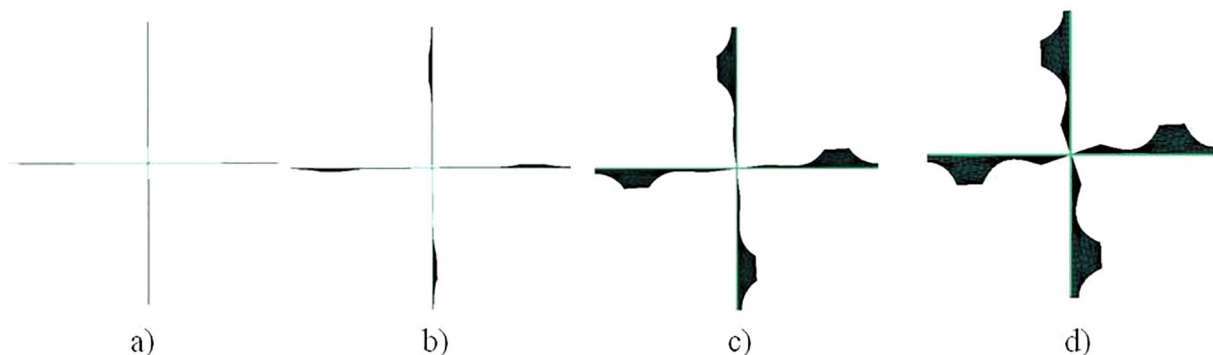
Fig. 12. FEM renders of design 2 struts showing the transition through instability.

**Table 5**
Comparison between the designed cores and references of similar materials found in literature.

| References | Core type | Base material | $\rho_s$ ( kg m$^{-3}$) | $\bar{\rho}$ (%) | E/$\rho$ (10$^6$ m$^2$ s$^{-2}$) | σ/$\rho$ (10$^3$ m$^2$ s$^{-2}$) |
|---|---|---|---|---|---|---|
| [3] | *Inco® foam* | Ni open cell | 8660 | 3.0 | 1.53 | 2.31 |
| | *Alporas® foam* | Al closed cell | 2500 | 8.0 | 2 | 6.5 |
| | *Alulight® foam* | Al closed cell | 2850 | 10.0 | 5.67 | 6.3 |
| | *ERG® foam* | Al open cell | 2500 | 5.0 | 0.38 | 5.25 |
| | *Cymat® foam* | Al-SiC closed cell | 2800 | 2.0 | 0.29 | 0.57 |
| [9] | Pyramidal truss lattice | Laminate 0/90° CFRP | 1440 | 3.5 | 4.96 | 99.2 |
| | | | | 3.0 | 5.21 | 92.5 |
| [10] | Square-honeycomb | Woven 0/90° CFRP | 1370 | 2.5 | 9.92 | 22.95 |
| | | | | 5.0 | 12.43 | 76.5 |
| | | | | 10.0 | 16.58 | 78.4 |
| [10] | Hybrid pyramidal lattice | Braided CFRP | 1450 | 3.0 | 1.15 | 22.99 |
| [16] | Square-honeycomb | AISI 304 | 7980 | 3.0 | 10.23 | 18.08 |
| | HexWeb ® | 3003 Al-alloy | 2800 | 3.0 | 1.31 | 6.57 |
| [26] | Square collinear truss lattice | Ti–6Al–4V-coated SiC (TMC) | 3930 | 9.6 | 9.7 | 81.11 |
| | Diamond collinear truss lattice | | | 9.6 | 18.41 | 66.45 |
| [31] | Tetrahedral truss lattice | Age-hardened AA 6061 | 2700 | 3.0 | 1.99 | 50.24 |
| | | | | 3.7 | 2.77 | 61.26 |
| [32] | Prismatic diamond | AISI 304 | 7980 | 8.0 | 3.03 | 8.56 |
| | Prismatic corrugated | | | 3.6 | 3.11 | 6.63 |
| [33] | BCC micro lattice block | EOS Ti6Al4V | 4410 | 5.6 | 0.31 | 16.76 |
| [34] | Hexagonal honeycombs | Woven Kevlar/914 | 1380 | 4.2 | 0.18 | 9.44 |
| | Auxetic honeycombs | | | 2.4 | 0.24 | 13.86 |
| Present work | Design 1 ULW hybrid | Laminate 0/90° CFRP | 1300 | 3.5 | 15.82 | 49.01 |

Notes: $\rho_s$ = density of base material.

## Appendix A. Supplementary data

Supplementary data associated with this article can be found, in the online version, at http://dx.doi.org/10.1016/j.compstruct.2018.03.065.

## References

[1] Petrone G, et al. Behavior of fibre-reinforced honeycomb core under low velocity impact loading. Compos Struct 2013;100:356–62.
[2] Zhang J, Ashby MF. The out-of-plane properties of honeycombs. Int J Mech Sci 1992;34:475–89.
[3] Ashby MF, Evans A, Fleck N, Gibson L, Hutchinson J, Wadley H. Metal foams: a design guide: Butterworth-Heinemann, Oxford, UK, ISBN 0-7506-7219-6, Published 2000, Hardback, 251 pp. Mater Des 2002;23:119.
[4] Petrone G, D'Alessandro V, Franco F, Mace B, De Rosa S. Modal characterisation of recyclable foam sandwich panels. Compos Struct 2014;113:362–8.
[5] D'Alessandro V, Petrone G, De Rosa S, Franco F. Modelling of aluminium foam sandwich panels. Smart Struct Syst 2014;13:615–36.
[6] Gibson Lorna J, Ashby Michael F. Cellular solids structure and properties. Cambridge University Press; 1999.
[7] Ashby MF. The properties of foams and lattices. Philos Trans R Soc A 2006;364:15–30.
[8] Wadley HN. Multifunctional periodic cellular metals. Philos Trans R Soc London A 2006;364:31–68.
[9] Finnegan K, Kooistra G, Wadley HN, Deshpande V. The compressive response of carbon fiber composite pyramidal truss sandwich cores. Int J Mater Res 2007;98:1264–72.
[10] Russell B, Deshpande V, Wadley H. Quasistatic deformation and failure modes of composite square honeycombs. J Mech Mater Struct 2008;3:1315–40.
[11] Vitale JP, Francucci G, Xiong J, Stocchi A. Failure mode maps of natural and synthetic fiber reinforced composite sandwich panels. Compos A Appl Sci Manuf 2017;94:217–25.
[12] George T, Deshpande VS, Sharp K, Wadley HNG. Hybrid core carbon fiber composite sandwich panels: Fabrication and mechanical response. Compos Struct 2014;108:696–710.
[13] NASA. Game changing development program, ultra-lightweightcore materials for efficient load-bearing composite sandwich structures. Washington, DC: National Aeronautics and Space Administration (NASA) Headquarters; 2014.
[14] Ashby M, Brechet Y. Designing hybrid materials. Acta Mater 2003;51:5801–21.
[15] Mozafari H, Khatami S, Molatefi H, Crupi V, Epasto G, Guglielmino E. Finite element analysis of foam-filled honeycomb structures under impact loading and crashworthiness design. Int J Crashworthiness 2016;21:148–60.
[16] Côté F, Deshpande VS, Fleck NA, Evans AG. The out-of-plane compressive behavior of metallic honeycombs. Mater Sci Eng, A 2004;380:272–80.
[17] Xiong J, Ma L, Stocchi A, Yang J, Wu L, Pan S. Bending response of carbon fiber composite sandwich beams with three dimensional honeycomb cores. Compos Struct 2014;108:234–42.
[18] Cote F, Deshpande V, Fleck N. The shear response of metallic square honeycombs. J Mech Mater Struct 2006;1:1281–99.
[19] Rosen BW. Mechanics of composite strengthening. Fiber Composite Materials. Metals Park, OH: American Society for Metals; 1965. p. 37.
[20] Argon AS. Fracture of composites. Treat Mater Sci Technol 1972;1:79–114.
[21] Budiansky B. Micromechanics. Comput Struct 1983;16:3–12.
[22] Budiansky B, Fleck N. Compressive failure of fibre composites. J Mech Phys Solids 1993;41:183–211.
[23] Timoshenko S, Gere J. Theory of elastic stability. New York: McGraw Hill; 1963. 2nd ed.
[24] Ericksen WS, March HW. Compressive buckling of sandwich panels having dissimilar facings of unequal thickness. Madison, WI: Forest Products Laboratory; 1958. Report 1583-B.
[25] Hutton DV. Fundamentals of finite element analysis. 1st ed. New York: McGraw Hill; 2004.
[26] Inc SPS. FEMAP – Finite Element Modeling and Post processing, Logo, Germany: 2011; Version 10.3.
[27] 364M-05 A-CC. Standard test method for flat wise compressive properties of sandwich cores West Conshohocken, PA 19428–2959, USA; 2000.
[28] Hibbitt K and Sorensen Inc.. ABAQUS analysis user's manual. Pawtucket, RI, USA: Hibbitt, Karlsson & Sorensen Inc; 2004. Version 6.4.
[29] Evans A, Hutchinson J, Ashby M. Multifunctionality of cellular metal systems. Prog Mater Sci 1998;43:171–221.
[30] Moongkhamklang P, Deshpande VS, Wadley HNG. The compressive and shear response of titanium matrix composite lattice structures. Acta Mater 2010;58:2822–35.
[31] Kooistra G, Deshpande V, Wadley H. Compressive behavior of age hardenable tetrahedral lattice truss structures made from aluminium. Acta Mater 2004;52:4229–37.
[32] Côté F, Deshpande VS, Fleck NA, Evans AG. The compressive and shear responses of corrugated and diamond lattice materials. Int J Solids Struct 2006;43:6220–42.
[33] Crupi V, Kara E, Epasto G, Guglielmino E, Aykul H. Static behavior of lattice structures produced via direct metal laser sintering technology. Mater Des 2017;135:246–56.
[34] Hou Y, Neville R, Scarpa F, Remillat C, Gu B, Ruzzene M. Graded conventional-auxetic Kirigami sandwich structures: Flatwise compression and edgewise loading. Compos B Eng 2014;59:33–42.